JACS
JOURNAL OF THE AMERICAN CHEMICAL SOCIETY
Article
pubs.acs.org/JACS

Perylenediimide-Based Donor–Acceptor Dyads and Triads: Impact of Molecular Architecture on Self-Assembling Properties

Pierre-Olivier Schwartz,[†] Laure Biniek,[‡] Elena Zaborova,[§] Benoît Heinrich,[†] Martin Brinkmann,[‡] Nicolas Leclerc,[§] and Stéphane Méry*[,†]

[†]Institut de Physique et de Chimie des Matériaux de Strasbourg, UMR 7504, CNRS, Université de Strasbourg, 23 rue du Loess, BP 43, 67034 Strasbourg, Cedex 2, France

[‡]Institut Charles Sadron, UPR22 CNRS, 23 rue du Loess, BP 84047, 67034 Strasbourg Cedex 2, France

[§]Institut de Chimie et Procédés pour l'Energie, l'Environnement et la Santé, UMR 7515, CNRS, Université de Strasbourg, ECPM, 25 rue Becquerel, 67087 Strasbourg Cedex 2, France

Supporting Information

ABSTRACT: Perylenediimide-based donor–acceptor co-oligomers are particularly attractive in plastic electronics because of their unique electro-active properties that can be tuned by proper chemical engineering. Herein, a new class of co-oligomers has been synthesized with a dyad structure (AD) or a triad structure (DAD and ADA) in order to understand the correlations between the co-oligomer molecular architecture and the structures formed by self-assembly in thin films. The acceptor block A is a perylene tetracarboxyl diimide (PDI), whereas the donor block D is made of a combination of thiophene, fluorene, and 2,1,3-benzothiadiazole derivatives. D and A blocks are linked by a short and flexible ethylene spacer to ease self-assembling in thin films. Structural studies using small and wide X-ray diffraction and transmission electron microscopy demonstrate that AD and ADA lamellae are made of a double layer of co-oligomers with overlapping and strongly π-stacked PDI units because the sectional area of the PDI is about half that of the donor block. These structural models allow rationalizing the absence of organization for the DAD co-oligomer and therefore to draw general rules for the design of PDI-based dyads and triads with proper self-assembling properties of use in organic electronics.

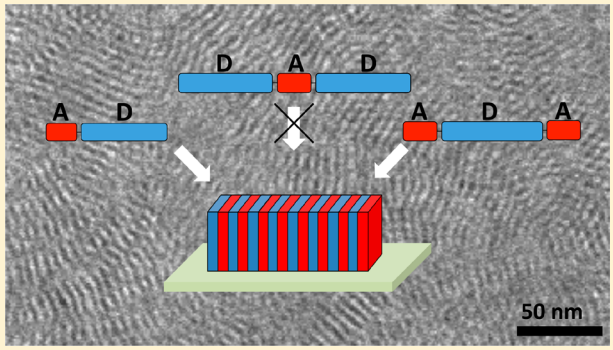

1. INTRODUCTION

Nanostructured 3D morphologies composed of electronically active constituents have gained interest in the field of organic electronic.[1−3] In particular organic solar cells with a well-ordered phase-separated donor and acceptor morphology, i.e. a so-called nanostructured D−A bulk heterojunction has been proposed as an "ideal structure", leading to OPV devices with enhanced efficiency and stability.[4,5] Generating sub-10 nm-sized donor and acceptor domains with a large interfacial area is expected to ease exciton separation, whereas a bicontinuous "percolation" network of the two components may improve charge-carrier conduction and extraction from the active layer to the electrodes.[6] Nanometer-scaled domains are also required because of the limited exciton diffusion length in organic thin films.[7] Ordered D and A arrays are also promising candidates for organic field effect transistors (OFETs) devices, since they could intrinsically exhibit an ambipolar charge transport through a bicontinuous *p*-type and *n*-type network. Various strategies were proposed to prepare thin films that fulfill all these requirements. They can be classified into two major categories: (i) methods based on chemical engineering that exploit the self-assembling properties of donor–acceptor (macro)molecular systems e.g., block copolymers[8] or co-oligomers[9,10] (including low-molecular weight compounds)[11−13] and (ii) physicochemical methods that use specific thin film processing methods e.g. nanoimprint lithography[14] or template-based methods.[15] While the latter methods seem very promising in terms of cost, reproducibility and large-scale integration, exploiting the self-assembling of precisely designed donor–acceptor block co-oligomers is of particular interest as the preparation methods may be facilitated by the intrinsic self-assembling properties of the co-oligomers.

Several teams have investigated the donor–acceptor block (D−A) copolymer approach implying the synthesis of a macromolecule where an electron donor and an electron acceptor block are chemically bound.[16] For many copolymers, the acceptor block was made of pendant fullerene C_{60}. However, in the past decade, perylenediimide (PDI) appeared as an interesting alternative acceptor unit to C_{60} in OPV devices.[8d−h] Many macromolecular architectures using PDI were synthesized and interesting properties such as *n*-type

Received: January 7, 2014
Published: March 27, 2014

dx.doi.org/10.1021/ja4129108 | J. Am. Chem. Soc. 2014, 136, 5981−5992

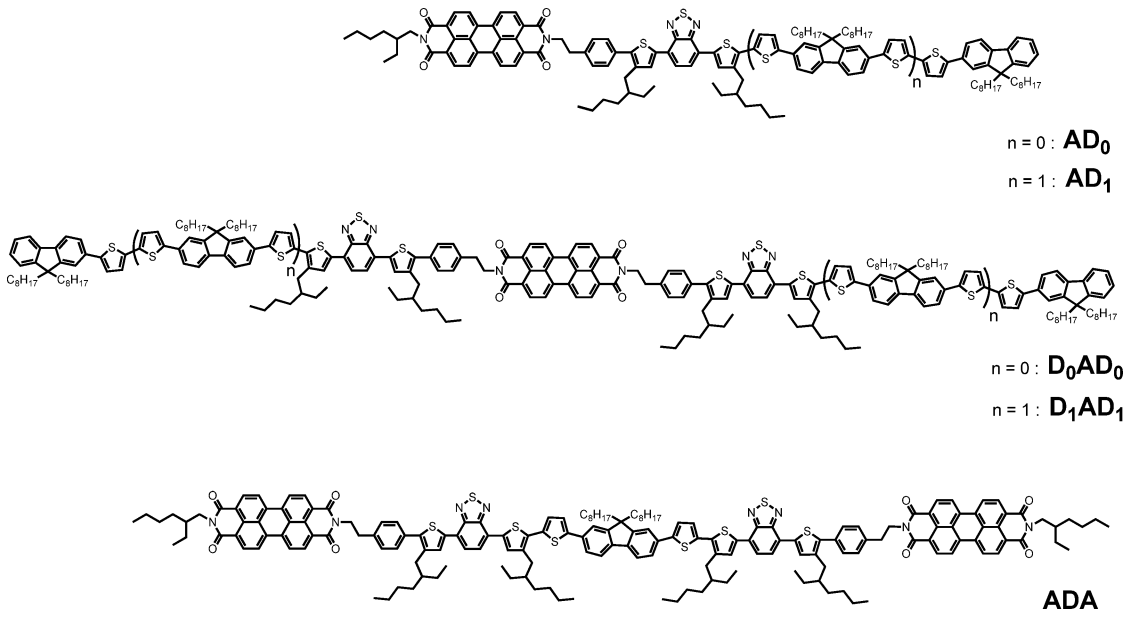

Figure 1. Chemical structure of the donor−acceptor block co-oligomers categorized into the three molecular architectures: AD_n, D_nAD_n and ADA.

transport and OPV activity were demonstrated.[17] In particular, D−A copolymers based on perylenediimides have recently gained high interest because of the combination of remarkable self-assembling properties along with a strong *n*-type charge transport.[8g,h] More generally, D−A copolymers have been used as active layers as well as stabilizers of donor/acceptor blends, but lead to rather limited charge transport and photovoltaic properties in thin films.[18]

One possible way to improve the block copolymer approach consists in the design of co-oligomers with a precise composition and molecular architecture avoiding, in particular, the issues of polydispersity and chemical purity inherent to copolymer. Recently, Y. Geng et al. demonstrated interesting OPV properties in thin film devices prepared from PDI-based oligomers forming lamellar mesophases with a perfect phase separation between donor and acceptor groups.[10c,d] The quality of the organization was found to be significantly improved by increasing the donor block length and by using solvent-vapor annealing to improve the film morphology. In these reports, however, only a series of oligomers of dyad architecture (AD) was investigated. Derived from the block co-oligomer approach, one has to mention the large number of low-molecular weight systems reported in the literature which are made of a "small" donor conjugated unit (<800 Da) covalently linked to a C_{60},[11] peryleneimide[12,13] or other acceptor unit,[19] into dyad or triad architectures. Only a few systems, however, could successfully lead to microphase separation of the blocks clearly leading to self-assembling into 3-D supramolecular D/A arrays.[11b−d,13,18] Liquid crystals seem to constitute a promising approach in that direction.[10c,d,11b,c,13a,g] With low-molecular weight systems, however, the small size of the electro-active species does represent a challenge to build up well-defined D and A channels over large-length scales to ease ambipolar charge transport.[11b,c,12f,13]

Herein we report the syntheses and the physicochemical properties of a series of donor−acceptor block co-oligomers of different molecular architectures within dyad (AD) and triad (ADA and DAD) systems. The donor block length has been only slightly varied to remain in the range of moderate molecular weight systems. The aim of this contribution is to investigate the structure−property relationship of these materials with particular emphasis on spectroscopic, thermal, and structural properties. A careful look will be brought to the molecular architecture dependence of the material organization, by means of X-ray diffraction studies (powder and GIWAXS) and electron microscopy investigation (TEM).

2. RESULTS AND DISCUSSION

Molecular Design and Synthesis. We have designed new molecular structures based on the approach of monodisperse block co-oligomers including both electron-acceptor (A) and electron donor blocks (D). Various molecular architectures e.g. AD, DAD and ADA (Figure 1) are prepared by assembling properly these two blocks.

The studied co-oligomers are made of the association of several chemical units: perylene tetracarboxyl diimides (PDI), thiophene, fluorene, and 2,1,3-benzothiadiazole derivatives (Figure 1). PDI presents an *n*-type character (A), while the other units compose the *p*-type block (D). PDI is made of a large aromatic macrocycle providing strong $\pi-\pi$ interactions that is the primary force to drive the formation of stacked structures.[20] The thienofluorene building block can be seen as a rigid conjugated rod, which incidentally showed its ability to produce mesophases when substituted by appropriate alkyl chains.[21] Its association with PDI was therefore expected to promote the formation of a lamellar organization with segregated D and A domains. This assumption was recently demonstrated in the case of the AD molecular architecture.[10c,d] The electron-deficient thiophene−benzothiadiazole−thiophene (TBzT) moiety has been included in the donor block with the intent of lowering the energy bandgap of the donor block by decreasing its LUMO level and red-shifting its absorption spectrum.[22] Finally, the covalent bonding of the donor block by N-substitution of the PDI core ensures an electronic disconnection between both blocks. In our systems, a nonconjugated ethylene linker is inserted between the D and A blocks to impede the direct charge recombination.[13c] It is also expected to bring some flexibility between both blocks to

dx.doi.org/10.1021/ja4129108 | J. Am. Chem. Soc. 2014, 136, 5981−5992

Scheme 1. Synthetic Pathway for the Preparation of the Amine-Ended Donor Blocks (D_0, D_1, and D) with Their Subsequent Coupling to the PDI unit, To Provide the Donor−Acceptor Block-*co*-Oligomers of Different Molecular Architectures (AD_n, D_nAD_n and ADA)

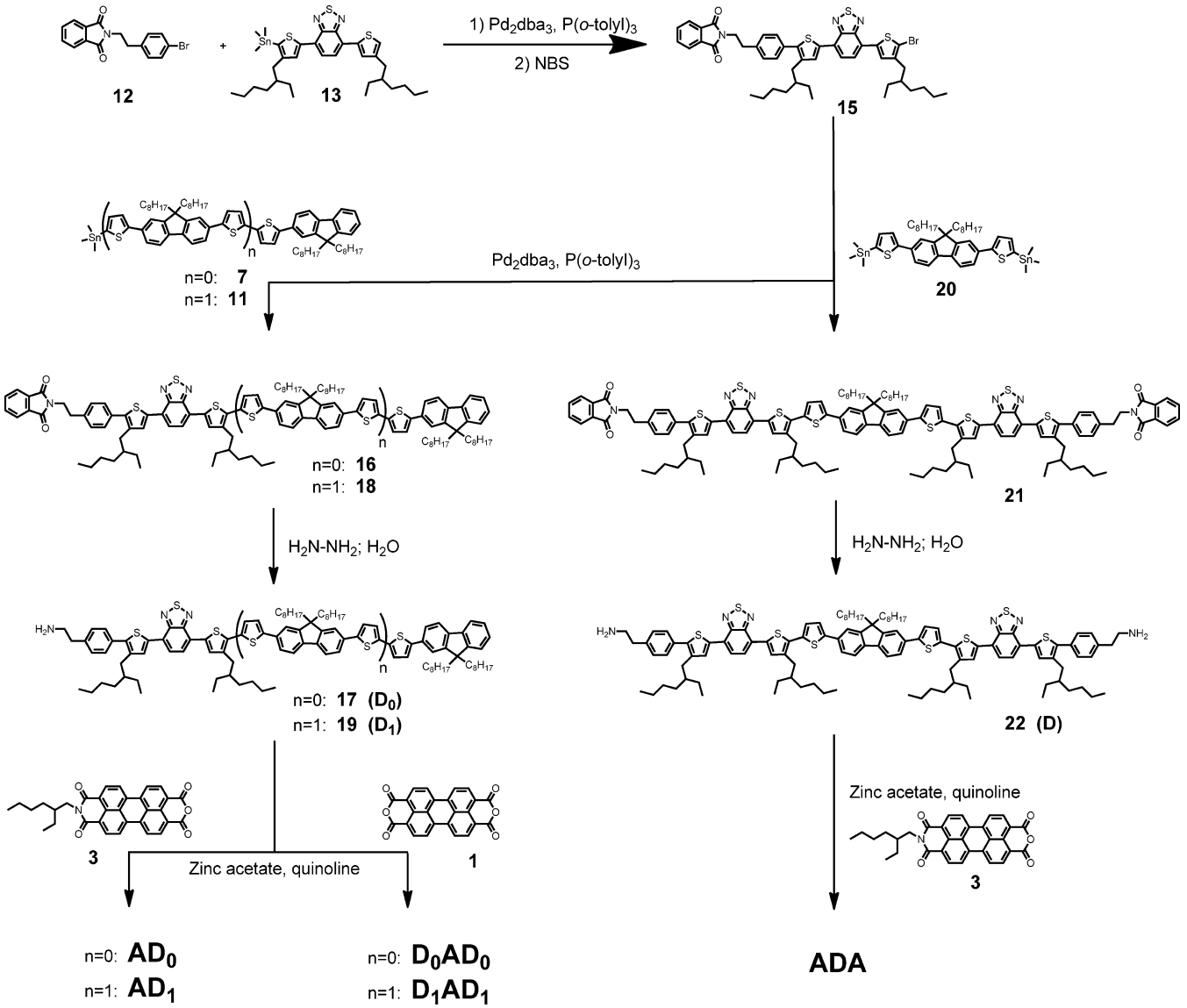

favor their respective packing. Moreover, this linker is expected to be short enough to prevent the D and A backfolding, already noticed for other systems with longer linkers,[23] which indeed is detrimental for the formation of nanostructures with segregated D and A domains.

Finally the choice of the solubilizing side chains, necessary to process these materials from solution, is also extremely influential for the material organization and consequently the optoelectronic properties.[24] In our case, we decided to use linear octyl chains on the fluorene moieties and 2-ethylhexyl-ramified chains on the PDI cores (when asymmetrized) and on thiophene units adjacent to the benzothiadiazole. Ethylhexyl side chains were chosen because of their higher solubilizing capability with respect to that of their linear counterparts.

All oligomers were synthesized using the same two-step strategy (Scheme 1). First, the whole donor blocks bearing an amine group at one end (for the AD and DAD architectures) or at the two ends (for the ADA architecture) were synthesized by using a convergent approach. These donor blocks were then connected to the carboxylic anhydride functionality of the PDI acceptor block, via an imidation reaction, to prepare the final dyads and triads. The synthetic routes are outlined in Scheme 1, while all detailed procedures are given in Supporting Information (SI).

For the AD and DAD architecture, the donor block length was slightly varied by adding a thiophene−di(octyl)fluorene−thiophene segment to the starting compounds AD_0 and D_0AD_0, as to obtain the AD_1 and D_1AD_1 co-oligomers, respectively. The lengthening of the donor block was not attempted on the ADA triad because of its poor solubility and processability due to the presence of two highly aggregating PDI units.

The electron-acceptor blocks **3** of the ADA triad and AD_n dyads are similar and required a previous asymmetrization step which was carried out according to the work of Bock et al.[25] In the case of the D_nAD_n triad, the commercially available perylene-3,4,9,10-tetracarboxylic dianhydride (PTCDA) **1** was directly used.

dx.doi.org/10.1021/ja4129108 | J. Am. Chem. Soc. 2014, 136, 5981−5992

Scheme 2. Chemical Structure of the Dyad AD_{0T}

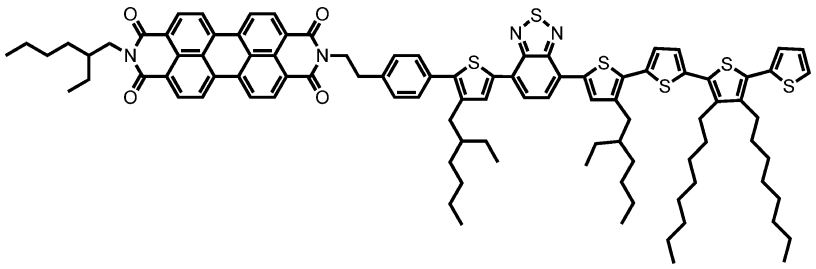

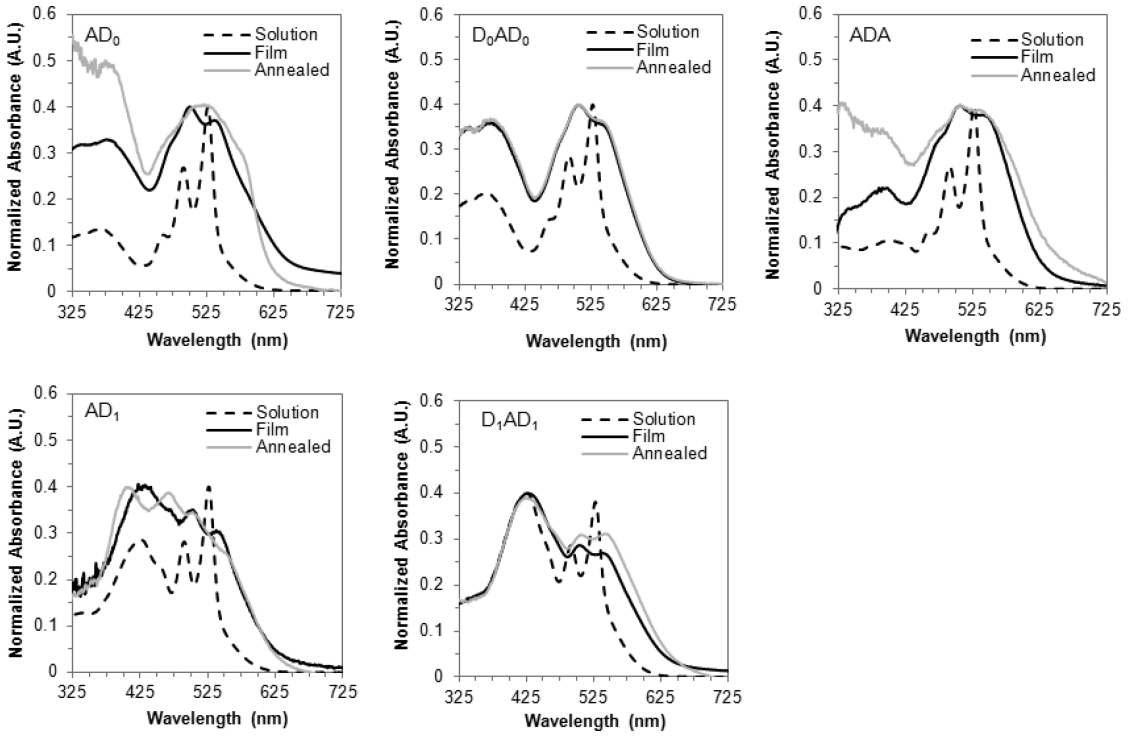

Figure 2. Normalized UV−vis absorption spectra of the co-oligomers in $CHCl_3$ (dashed line), in thin film (plain black line), and in post-annealed film (gray line).

The synthesis of electron-donor blocks is identical for that of the D_nAD_n and AD_n series (Scheme 1). It starts with the synthesis of the electron-deficient TBzT derivative **15** bearing at one end a phthalimide moiety, precursor to the amine functionality and at the other end, a bromine atom for subsequent adjunction of a thienofluorene moiety. This intermediate compound (**15**) was obtained from successive reaction steps, involving a Stille cross-coupling reaction between *N*-bromophenethyl(phthalimide) **12** and the stannylated TBzT derivative **13**,[23] and then a bromination using NBS. All reaction steps were achieved in rather high yield except the Stille cross-coupling reaction (~60% yield), most likely due to the steric hindrance caused by the ethylhexyl chain adjacent to the stannylated position in **13**. In a next step, **15** was cross-coupled with the thienofluorene derivative **7** or **11** to produce the phthalimide-ended donor blocks **16** or **18** of different length (n = 0 or 1, respectively) in 78−90% yield. The latter were obtained from multiple reaction steps (85−95% yield each), involving trimethylstannylation (via either a H/Li or Br/Li exchange), bromination (NBS), and Stille cross-coupling reactions. The whole amino-ended donor blocks **17** (D_0) and **19** (D_1) were finally obtained after cleavage of the phthalimide protecting group by hydrazinolysis in quantitative yield. These donor blocks were used without further purification for the last imidation step with the perylene carboxylic anhydride **1** or dianhydride **3** to provide the targeted dyads (AD_0 and AD_1) or triads (D_0AD_0 and D_1AD_1), respectively. These final reactions were carried out in quinoline at 200 °C in the presence of zinc acetate. Several purification steps by column chromatography on silica gel (petroleum ether/CH_2Cl_2) were required to afford pure oligomers. They were obtained in good yields (around 80%) as purple solids and characterized by NMR and Maldi-TOF analyses.

In the case of the ADA triad, we have synthesized a specific donor block composed of two amino-functionalized TBzT moieties **22** (D). This donor block synthesis was performed by using a Stille cross-coupling reaction between the TBzT derivative **15** and the bis-stannylated thienofluorene **20**,[26] followed by a cleavage (hydrazinolysis) of the phthalimide protecting groups. The final ADA triad was obtained from a double imidation reaction between the bis-amino derivative **22** and the perylene dicarboxylic anhydride **1** with a limited yield of 26%. This low yield is ascribed to the increased amount of byproducts and the poor solubility of the final compound. Proper purification by several column chromatographies on

dx.doi.org/10.1021/ja4129108 | J. Am. Chem. Soc. 2014, 136, 5981−5992

Table 1. Optical, Electrochemical and Thermal Characterization Data of the Co-oligomers

Oligomers	$E_{g\ opt}$ (eV)[a]	E_{ox} Onset D (V)[b]	E_{red} Onset A (V)[b]	HOMO D (eV)[b]	LUMO A (eV)	T_g (°C)	T_{iso} /°C (ΔH/J·g^{-1})[c]	T_c /°C (ΔH/J·g^{-1})[c]	T_{deg} (°C)[d]
AD_0	1.97	0.79	−0.50	−5.54	−4.25	–	223 (17.97)	209 (18.91)	405
AD_1	1.96	0.77	−0.50	−5.52	−4.25	–	205 (11.42)	194 (11.84)	350
ADA	1.96	0.94	−0.85	−5.69	−3.90	–	269 (17.25)	240 (15.61)	320
D_0AD_0	1.97	0.73	−0.50	−5.48	−4.25	38	–	–	330
D_1AD_1	1.96	0.74	−0.50	−5.49	−4.25	53	–	–	400

[a]Optical band gap estimated from the absorption onset of thin films. [b]Oxidative (E_{ox} and HOMO) and reductive (E_{red} and LUMO) contribution from the donor and acceptor block, respectively. All measurements were made in solution (CH_2Cl_2), except for ADA (solid film). [c]Onset isotropization and crystallization temperatures. [d]Calculated from the inflection point measurement.

silica gel (chloroform/methanol) provided the purple solid of ADA of good purity.

In order to evaluate the role of the thienofluorene unit on the molecular organization, another dyad (AD_{0T}) was also synthesized in which the thienofluorene was replaced by a terthiophene unit (Scheme 2). Both units similarly contain two linear octyl side chains. The synthetic pathway is reported in SI (Schemes S6 and S7). On the basis of the thin film morphology analysis performed by TEM, the structural organization of AD_{0T} will be compared with the one of AD_0.

Spectroscopic and Redox Properties. The UV−visible absorption spectra of the co-oligomers recorded in solution (in chloroform) and in thin films (doctor-bladed from solution at 45 °C) before and after post-annealing treatment (close to the melting) are presented in Figure 2. In solution, the absorption spectra of all co-oligomers are dominated by the characteristic vibronic structure of the PDI core with components at 465, 495, and 530 nm. The donor contribution is represented by two bands, one in the range 325−425 nm, whose position is correlated to the donor length conjugation, and the second one, centered at about 450 nm which extends beyond the absorption range of PDI, to 600 nm. This latter contribution can be correlated to the electron-deficient benzothiadiazole-based part of the donor group (see Figure S1 in SI). In thin films, the contribution of the PDI block broadens as a consequence of the excitonic coupling in the solid state with an additional red-shifted contribution seen as a shoulder at $\lambda \approx 600$ nm for AD_0. After annealing of the films at a temperature close to the isotropization temperature, a clear variation of the fine structure of the absorption of the PDI block is observed for all the oligomers, except for D_0AD_0 which remains unchanged whatever the thermal post-treatment applied. This is in agreement with the DSC results showing a clear first-order phase transition for AD_0, AD_1, and ADA upon cooling from the melt, whereas such transition is observed neither for D_0AD_0 nor for D_1AD_1 (vide infra).

As a first investigation of the excited states, the emission spectra in solution (10^{-6} mol L^{-1}) were recorded for one representative material, the dyad AD_1 (Figure S2 in SI). Upon excitation of AD_1 at 400 nm, a quasi-quantitative quenching of fluorescence is observed. This implies the exciton dissociation via a charge transfer from the donor to the acceptor block and no radiative recombination of separated charges. This implies also that the $(-(CH_2)_2-)$ linker does not prevent the intramolecular charge transfer, contrary to previous observations in another series of block co-oligomers made of hexa-*peri*-hexabenzocoronene and PDI units.[13c] Similar behavior was observed for all our synthesized co-oligomers (Figures S1−S4 in SI). By comparison, excitation of the isolated donor block (not connected to A) at the same wavelength (400 nm), gives rise to a typical emission band centered at about 650 nm. More remarkable is the almost complete fluorescence quenching observed whatever the excitation wavelength selected. Thus, upon excitation at 530 and 570 nm, an efficient quenching of fluorescence was observed (Figures S1−S4 in SI). At such wavelengths, only the electron-deficient benzothiadiazole-based part of the donor block and the PDI acceptor block is absorbing. These results point at an efficient exciton dissociation in those block co-oligomers, even in diluted solution.

The electrochemical properties of the co-oligomers were probed by cyclic voltammetry. Ferrocene was used as internal standard to convert the values obtained with Ag/Ag$^+$ reference to the saturated calomel electrode scale (SCE). In order to have an insight into the intrinsic electrochemical properties of our D−A block co-oligomers, the analyses were carried out in solution (methylene chloride) for all materials, except for ADA molecule. Due to its poor solubility in most organic solvents, ADA was only analyzed in the solid state, using acetonitrile as electrolytic support. Cyclic voltammograms are presented in the SI (Figures S5, S6, and S7), while the values are reported in Table 1.

All materials exhibited well-reversible oxidative and reductive processes. In solution, they displayed two successive reversible monoelectronic reduction waves around −0.50 V and −0.70 V, respectively, that are classically found for PDI (Figures S5 and S6 in SI). In the case of ADA in the solid state, the two-electron reduction occurs in a single wave at −0.85 V (Figure S7 in SI). It is not a particular feature since all our block co-oligomers show similar behaviors in the solid state. By using the NHE formal potential of −4.75 eV, LUMO levels of PDI blocks were calculated at −4.25 eV for AD_n dyads and D_nAD_n triads in solution, and at −3.90 eV for ADA triad in solid state. No oxidation of the PDI core could be observed in the range of measured voltages. Regarding the electron-donor blocks, we were able to determine the oxidative and reductive processes for all molecules. Similarly to the LUMO level of PDI, minor differences were observed in the HOMO levels of all molecules in solution. They all exhibited two oxidation waves in the range 0.7−1.1 V, corresponding to extracted HOMO levels ranging from −5.48 to −5.54 eV. The cathodic current increase observed for D_nAD_n triads in comparison with AD_n dyads confirms the bielectronic nature of those oxidative waves. This feature is the result of the presence of two decoupled electron donor blocks in one single D_nAD_n molecule. For all molecules, we were also able to measure a reduction process around −1.2 V, corresponding to the electron-donor blocks D_0 and D_1. Electrochemical band gaps of 1.9−2.0 eV were thus obtained for both donor blocks in solution, in good agreement with the band gaps measured in solid state for the pure electron-donor

dx.doi.org/10.1021/ja4129108 | J. Am. Chem. Soc. 2014, 136, 5981−5992

blocks. Regarding the electron-donor block of the ADA triad in solid state, similar voltammograms could be recorded with two oxidation waves and one reduction wave (Figure S7 in SI). Due to a shift of the first oxidation wave toward the higher potentials, a higher electrochemical band gap of 2.1 eV has been calculated. Although the block co-oligomers presented structural variations, the HOMO and LUMO levels were not significantly changed which implies that the imide group together with the flexible $(-(CH_2)_2-)$ linker between donor and acceptor blocks ensures adequate decoupling of electronic states of the blocks. This is in agreement with the absence of charge transfer (CT) band for co-oligomers in UV−vis spectra (diluted solution and thin films).

Thermal and Structural Properties. The thermal properties of the molecules have been characterized by thermogravimetric analysis (TGA), differential scanning calorimetry (DSC), and polarized optical microscopy (POM). First, all materials show a good thermal stability with a temperature of degradation occurring at $T_{deg} \geq 320$ °C (see Figures S8−S12 in SI and Table 1). As shown in Figure 3, the DSC thermograms

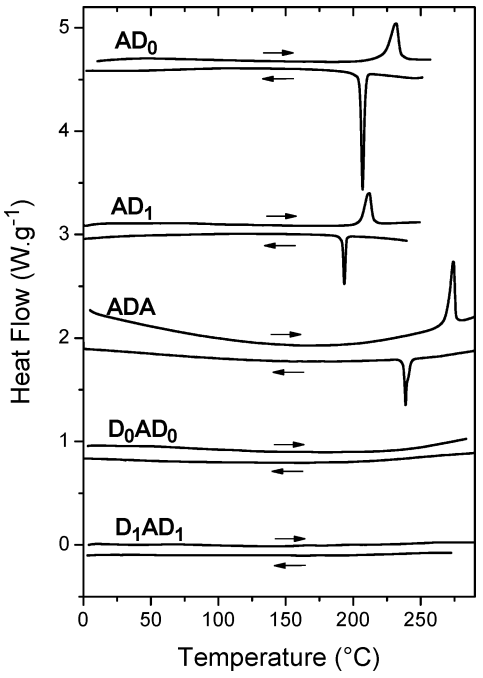

Figure 3. DSC thermograms of the co-oligomers (heating and cooling rates of 10 and 5 °C·min^{-1}, respectively).

show a first transition peak upon heating and cooling only for AD_0, AD_1, and ADA compounds, while no transition is detected for D_0AD_0 or D_1AD_1 besides a glass transition temperature (T_g). The peaks observed upon heating correspond to the transition to the isotropic liquid state (T_{iso}). These T_{iso} values are close for AD_0 and AD_1 (223 and 205 °C, respectively), while ADA exhibits the highest temperature (T_{iso} = 269 °C). The weak supercooling effect ($T_{iso} - T_c < 30$ °C) associated with the low enthalpy value of the transitions (<20 J·g^{-1}) suggested that the low-temperature phase in AD_n and ADA is a mesophase rather than a pure crystalline phase. This assumption is corroborated by POM observations from the pasty character of the birefringent texture found for AD_n and ADA materials. The mesomorphic nature of these compounds is further confirmed using X-rays analyses. In contrast, the amorphous-like character of D_0AD_0 and D_1AD_1 is confirmed by POM observation from the absence of birefringence in the whole temperature range explored from 20 to 300 °C.

In the pristine state, the five compounds give rise to small-angle X-ray scattering patterns characteristic of a segregated structure (see Figure S13 in SI). More exactly, the patterns contain a broad wide-angle scattering maximum at about 1.5 Å^{-1} (~4.5 Å) that overlaps a semi-broad scattering (~3.5 Å) due to distances between stacked PDI groups. The four compounds (AD_n and D_nAD_n series) exhibit, in the small and medium angle region, several broad reflections from an embryonic structure resulting from the microsegregation in separate domains of the lateral chains, the donor rigid parts and the PDI unit. For the triad ADA, the segregation is enhanced with respect to the dyads and leads to positional long-range order as indicated by a set of sharp reflections.

Most importantly, thermal annealing the oligomers is found to improve substantially the ordering of AD and ADA. Figure 4

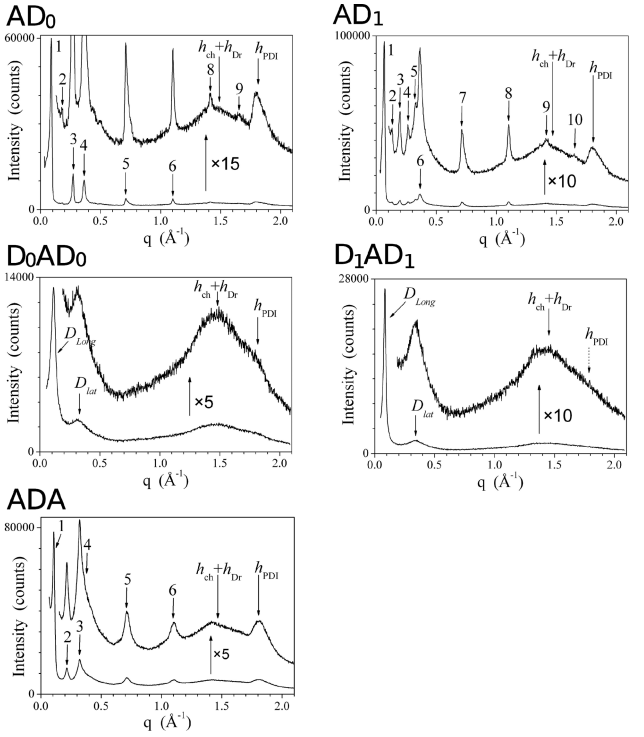

Figure 4. X-ray diffraction patterns of the series of co-oligomers obtained at room temperature after thermal annealing above 170 °C.

shows the characteristic powder X-ray diffractograms of the five oligomers (AD_0, AD_1, D_0AD_0, D_1AD_1, and ADA) recorded at room temperature after a melting or heating above 170 °C. Except for the DAD-based triads, all patterns exhibit the same sequence of (0 0 l) reflections at low angle corresponding to lamellar mesophases with long-range order. Lamellar periods for AD_0, AD_1, and ADA after annealing are 70.8, 96.5, and 58.8 Å, respectively. Further evidence of lamellar mesophases after melt-cooling is obtained by TEM (Figure 5 and Figure 7). In addition, all three co-oligomers (AD_0, AD_1, and ADA) show a set of at least five well-defined peaks with almost identical positions and intensities in the range 0.28 Å^{-1} < q < 1.85 Å^{-1}. This sequence of peaks characterizes the molecular packing of co-oligomers within the lamellae. More specifically, the quite broad peak at 1.80−1.88 Å^{-1} corresponds to the π-stacking of

dx.doi.org/10.1021/ja4129108 | J. Am. Chem. Soc. 2014, 136, 5981−5992

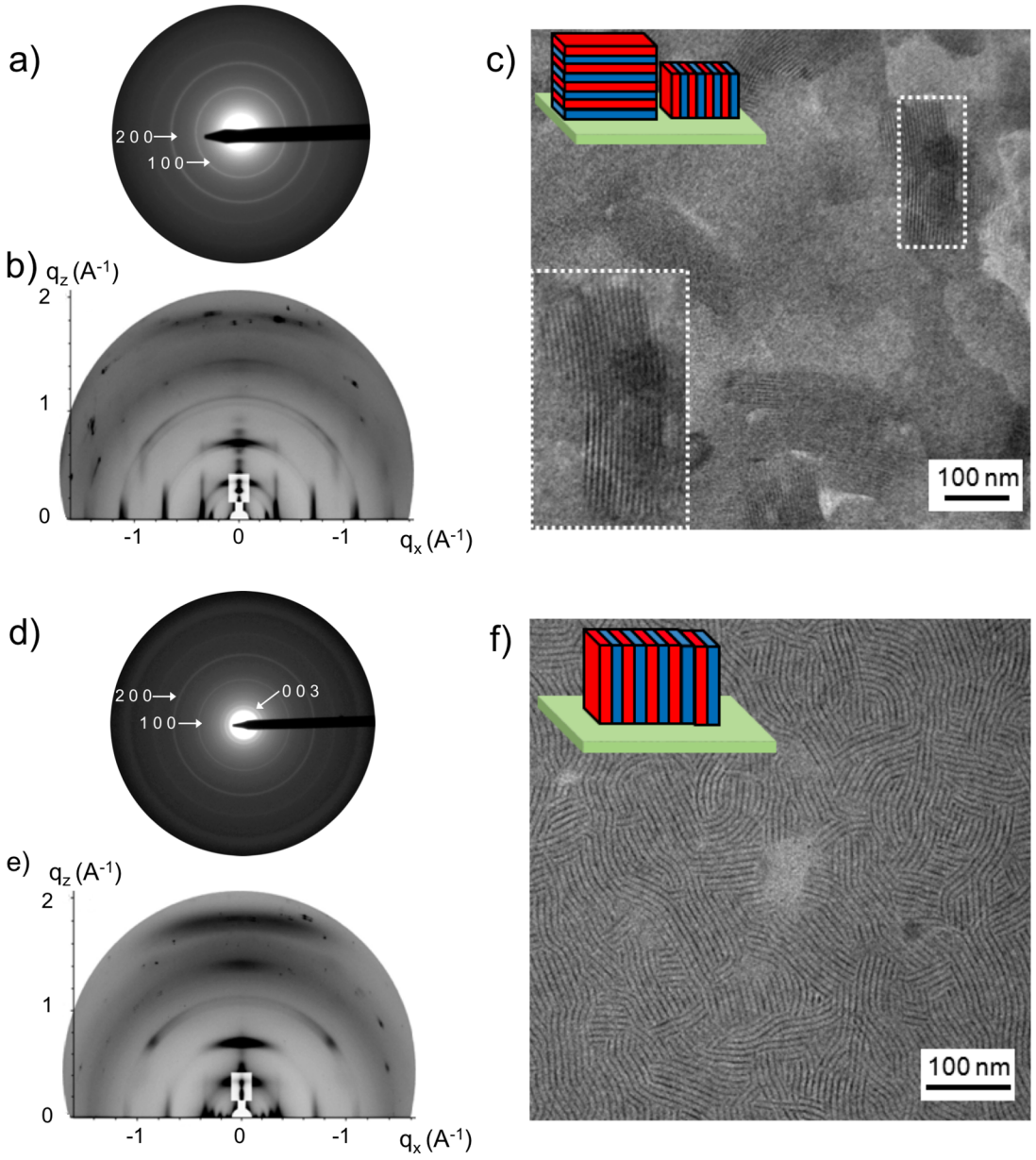

Figure 5. ED patterns (a and d), two-dimensional grazing incidence X-ray diffraction (GIWAXS) intensity maps (b and e), and TEM-BF images (c and f) of AD_0 (a,b,c) and AD_1 (d,e,f) thin films after annealing above the melting temperature. The insets represent the dominant orientation of the lamellae on the SiO_2 substrate. The inset in (c) highlights a set of standing lamellae also shown in an enlarged view in the lower left corner.

the PDI blocks, h_{PDI} (maximum at 3.5 Å).[27] The broad scattering maximum at 1.5 Å^{-1} comes from lateral distances between molten alkyl side chains (h_{ch}) and likely between rigid moieties of donor blocks segments (h_{Dr}). Additional peaks correspond to the reflections of the three-dimensional structure emerging from the segregation of alkyl chains and donor blocks.

Contrarily to AD_n and ADA compounds, both DAD derivatives exhibit, even after annealing, a poorly defined pattern (Figure 4). The latter is dominated by a slightly broadened peak corresponding to lamellar periods of 56 and 76 Å for D_0AD_0 and D_1AD_1, respectively, besides two broader peaks at 0.31 and 1.5 Å^{-1} coming from lateral distances between chains and rigid moieties. The absence of a clear h_{PDI} peak combined to the persistence of a quite sharp lamellar period (D_{Long}) shows that the layers of parallel packed molecules are preserved, but without the regular PDI stacks and only over intermediate correlation ranges (see Table 2). Finally, the lack of long-range order in D_0AD_0 and D_1AD_1 results in POM observation of textures, typical of an isotropic liquid, i.e. without birefringence in the liquefied-cooled thin films. In contrast to DAD-based triads, the ADA triad forms a lamellar mesophase already in the pristine state. However, this pristine lamellar structure differs from that obtained after melt-cooling (see Figure S14 in SI and Table 2). In particular, the lamellar period is 30% smaller in the pristine state. Above 100 °C the pristine structure gradually rearranges toward the stable lamellar mesophase, which is also the structure obtained in melt-cooled thin films. The sequence of peaks in the range 0.28 Å^{-1} < q < 1.85 Å^{-1} observed for ADA after annealing is almost identical to that observed for the AD_0 and AD_1 dyads, indicating a strong similarity in the molecular packing of the ADA triad and the AD_n compound series.

dx.doi.org/10.1021/ja4129108 | J. Am. Chem. Soc. 2014, 136, 5981−5992

Table 2. Mesomorphism and Structural Parameters of the Compound Series Annealed above 170 °C for about 1 h[a]

cmpd name	molecular length (Å)	phase and lattice parameters		ρ (g·cm^{-3})	molec areas	
					A_D[d]	A_{PDI}[e]
		orthorhombic phase[b]				
		a ; b ; c (Å)	V (Å)^3 (Z)			
AD_0	50	35.5 ; 7.43 ; 70.6	18600 (Z = 8)	1.14	65.9	33.0
AD_1	66	35.4 ; 7.44 ; 96.3	25400 (Z = 8)	1.13	65.8	32.9
ADA	86	35.2 ; 7.45 ; 117.8	30800 (Z = 8)	1.21	65.4	32.7
ADA (prist)	86	29.4 ; 12.7 ; 81.2	30400 (Z = 8)	1.23	94	47
		isotropic-like phase[c]				
		D_{1at} (ξ) (Å)	D_{Long}(ξ) (Å)			
D_0AD_0	84	21 (30)	56 (160)	*1.17*	*66*	*66*
D_1AD_1	116	18 (50)	76 (400)	*1.14*	*71*	*71*

[a]The structural parameters for both dyads and ADA triad have been determined considering the model proposed in Figure 8b and d. [b]a, b, c: lattice parameters; V: lattice volume; Z: number of molecules per lattice; ρ: density extracted from the unit cell parameters or calculated from reference density measurements (in italics). [c]D_{Long}: lamellar period; D_{1at}: periodicity from lateral packing; ξ: correlation length in Å extracted from the Scherrer formula. [d]A_D: molecular area per donor group (i.e., the area of the layer portion covered by a single group), as obtained from the ratio of molecular volume and either the parameter c or D_{Long}. [e]A_{PDI}: molecular area per PDI group.

Thin Films Morphology and Structure. TEM investigation of AD_0 and AD_1 dyads as-cast films do not give any indication for long-range order or structure. The situation changes upon melt-cooling of the samples. Figure 5 depicts the morphology and the ED and GIWAXS for thin films of AD_0 and AD_1 dyads after melt-cooling. The films of AD_0 consist of a majority of flat-lying lamellae with a typical terraced morphology. However, a small fraction of standing lamellae are also observed, and these areas give rise to a periodic fringed pattern characteristic of the lamellar mesophase with a period l = 70.6 Å. For the analogous AD_{0T} dyad, shown in Scheme 2, a similar terraced morphology was also evidenced by TEM and ED after melt-cooling (Figure 6). In strong contrast, the films

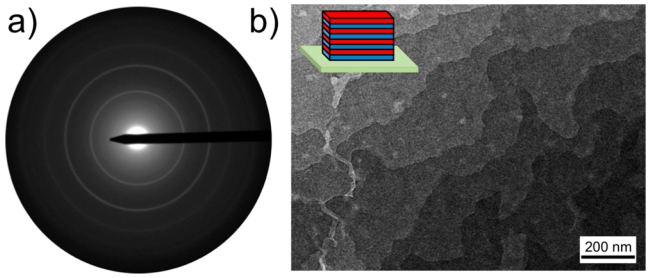

Figure 6. (a) ED pattern and (b) terrace-like morphology observed by BF-TEM of AD_{0T} thin film after annealing above the melting state.

of AD_1 consist essentially of standing lamellae as indicated by the observation of a periodic fringed pattern. The contrast in the TEM-BF images (Figure 5f) is attributed to the difference between the packing density of PDI and of the donor blocks. The sharp and dark lines are attributed to dense layers of PDI blocks, whereas the brighter zones correspond to the layers of donor blocks. The difference in lamellar orientation for AD_0 (and AD_{0T}) and AD_1 indicates that, for short donor blocks, the dyad molecules can stand up on the substrate upon annealing, whereas for AD_1 the molecular long axis remains in the plane of the substrate. These differences in morphology are confirmed by ED. Indeed, the characteristic (0 0 l) reflections are only seen in the case of AD_1, whereas for AD_0 (and AD_{0T}) the ED pattern shows exclusively the (h 0 0) reflections. The same analysis can be conducted for the GIWAXS patterns. If we consider the in-plane reflections (along q_x), one observes the (h 0 0) reflections with a weak (0 0 3) contribution for AD_0. Instead, for AD_1, the (0 0 l) reflections are dominant. Along q_z, the situation is reversed: for AD_0, the presence of both (h 0 0) and (0 0 l) reflections along q_z confirm the coexistence of both flat-on and edge-on oriented lamellae. For AD_1, the (h 0 0) reflections are very strong without any contribution from the (0 0 l) reflections along q_z.

The difference in molecular orientation in dyad films observed as a function of the donor block length has important implications regarding potential devices properties. Accordingly, in melt-cooled films, one can expect edge-on oriented lamellae with lying molecules of AD_1 to be more favorable for OPV applications with respect to AD_0 and AD_{0T} films consisting of terraced domains with standing molecules.

As previously demonstrated by XRD on pristine powders (Figure S14 in SI), the ADA triad presents enhanced ordering with a well-defined lamellar mesophase. This is confirmed by TEM observations on as-cast films prepared by doctor-blading. It is worth mentioning that for ADA triad, doctor-blading has been realized at 180 °C for solubility reasons. In this condition, a clear segregation of donor and acceptor blocks leads to a lamellar mesophase (Figure 7a). However, as seen in Figure 7c, after melt-cooling, the dimension of the domains is substantially increased and the contrast/sharpness of the lamellar morphology is strongly enhanced. The extension of long-range lamellar order is also evidenced by a strong increase of the intensity of the (0 0 l) reflections in the corresponding ED pattern (see Figure 7b and d).

In strong contrast to AD_n and ADA compounds, TEM investigations on D_0AD_0 and D_1AD_1 films did not show any evidence of long-range-ordering independently of the thermal annealing (see Figure S15 in SI).

Correlation between Molecular Packing and Molecular Architecture. The strong similarity in the XRD patterns of dyads based on different donor blocks (different lengths and chemical compositions) indicates that the self-organization of dyads into lamellar mesophases is mainly determined by the packing of the PDI blocks. Let us consider first the case of AD_0. For AD_0, the lamellar period lies between 1 and 2 times the length of the extended molecule. This suggests strongly that the lamellae involve two overlapping dyad molecules. This overlap may concern either the PDI block or the donor block. To discriminate between these two possibilities, we have to

dx.doi.org/10.1021/ja4129108 | J. Am. Chem. Soc. 2014, 136, 5981−5992

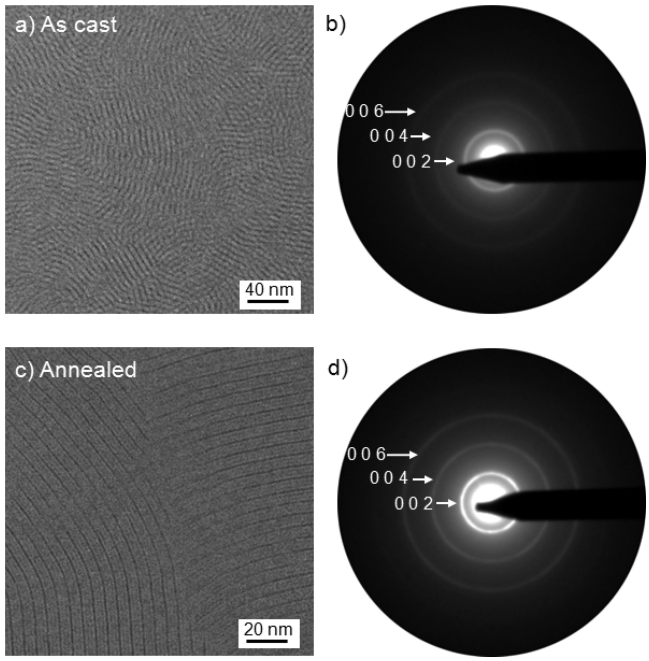

Figure 7. Comparison of TEM-BF images and low-angle ED patterns of as-cast (a and b) and annealed (c and d) ADA thin films.

consider the sectional areas of both blocks. The partial volumes of the donor and acceptor segments can be deduced from reference data and complementary measurements. They show that the sectional area of the donor groups including the molten lateral chains is at least 55 Å^2. This section largely exceeds the one of the stacked PDI of ~28.5 Å^2 as obtained from reference crystalline structures,[28] and it increases to roughly 30−32 Å^2 in mesophases.[29] In other words, the sectional area of the donor group is about twice that of the PDI block. This supports strongly the idea that the PDI blocks of dyad molecules are overlapping, but not the donor blocks. This overlapping of PDI blocks of two dyads in a lamella generates very dense planes of perfectly π-stacked PDI units with a short 3.5 Å stacking period as illustrated in Figure 8a,b. These dense planes of PDI blocks explain further the very strong contrast in the TEM-BF of the lamellae, the sharp and dark lines corresponding to the planes of densely stacked PDI units. The same reasoning holds also for the organization of the ADA triad with overlapping layers of PDI groups on either side of the donor block (see Figure 8c,d). Very likely, it is the presence of the flexible spacer between A and D units that gives sufficient freedom to the entire system to comply with the dense packing of PDI layers whatever the detailed structure of the D group (D_0, D_1, or D_{0T}). Such a flexible spacer allows to adjust the tilting of the D group within the unit cell. The net result of this is that both tilting and coiling of the lateral chains lead to a molecular area per PDI group of 33 Å^2 and thus to a molecular area per donor group around 66 Å^2 for all three investigated compounds (see Table 2).

Bridging PDI monolayers freeze the positions of neighboring co-oligomer molecules and donor moieties and then arrange laterally. Fluorene or thiophene moieties can give rise to a chevron packing, rather than face-to-face packing, which is moreover hindered by the bulky lateral chains. These segments are present in the three dyads and impose the chevron packing to the whole donor blocks and thus the *b* parameter of 7.4 Å. This value logically exceeds the natural face-to-face packing

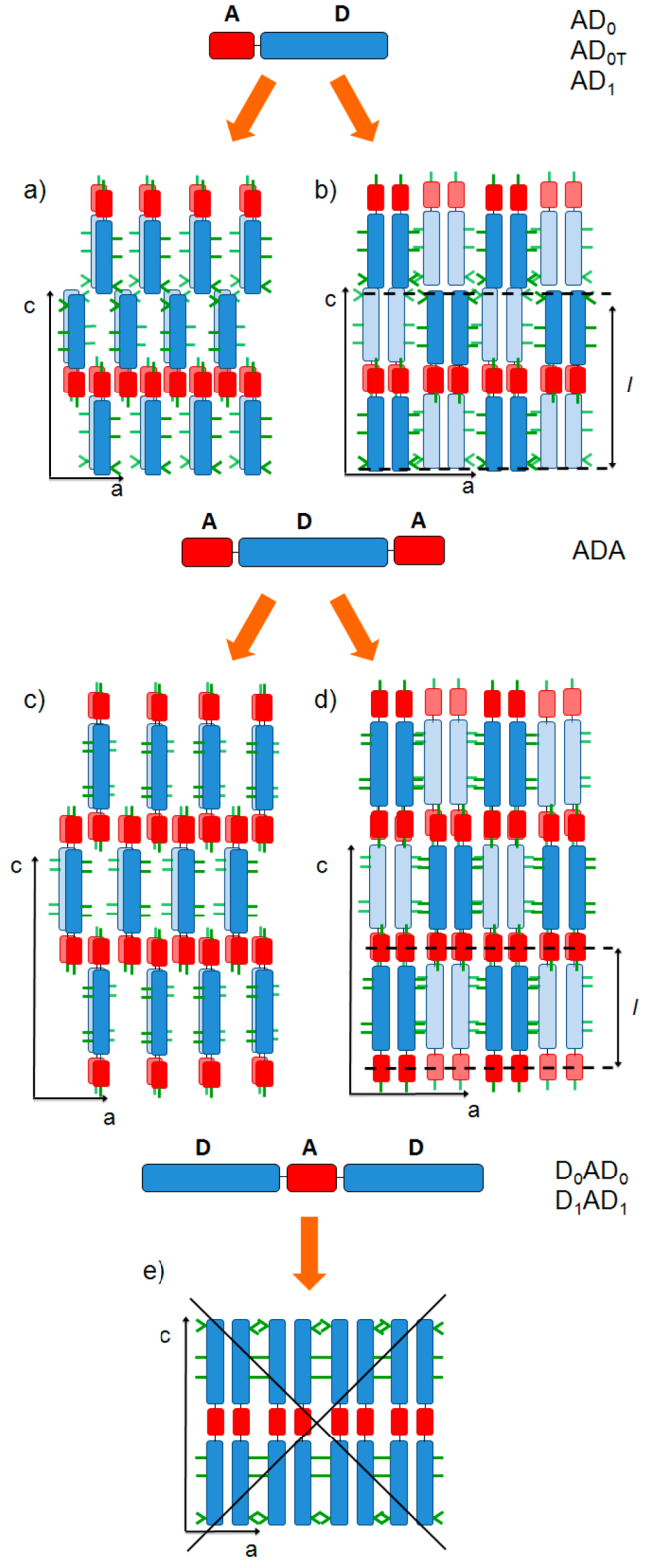

Figure 8. Schematic view of the two proposed models of organization of the AD and ADA based co-oligomers. A doubling of the **a** parameter is implied for models (b) and (d). The packing of DAD molecules, shown in (e), following the proposed models of ADA triad, is not possible because of the steric hindrance generated by the ethylhexyl side chains. PDI blocks are in red, donor blocks in blue, and alkyl side chains are in green. Donor blocks shown in dark blue are in an upper layer, whereas light-blue ones correspond to the layer beneath. *l* corresponds to the lamellar period.

dx.doi.org/10.1021/ja4129108 | J. Am. Chem. Soc. 2014, 136, 5981−5992

distance of PDI groups (~3.5 Å deduced from the h_{PDI} scattering), and the discrepancy needs to be compensated by small tilts of the stacked PDI groups. GIWAXS patterns confirm these tilts, since the π-stacking scattering maxima appear tilted about 15−20° from the **b** vector direction (see Figures 5b and e). Furthermore, the lamellae of donor moieties are interrupted by perpendicular layers of molten aliphatic chains (see Figure 8). The lateral periodicity coinciding with the parameter a = 35−35.5 Å involves the chains and rigid moieties of two donor blocks and therefore four PDI groups shared by two lamellae. The side-by-side packing of the PDI stacks then imposes a spacing of 8.8 Å per stack, close to values in crystalline phases (8.3 Å[28]). Except for the different c parameters related to the donor block lengths, the three dyads and the ADA triad just show the same annealed structures and similar geometrical parameters. As mentioned above, the ADA triad moreover shows a mesophase and long-range order already in the pristine state. The main specificities of the pristine geometry consist in a 40% reduced lamellar spacing and a 70% expansion along **b**, revealing an average 45° tilt of molecules from the **b** direction. As confirmed by the absence of all crossed reflections, the regular microsegregated layer alternation along ***a*** of the orthorhombic phase does not form natively, forcing rigid moieties to tilt. With the softening of the sample on first heat, this segregated structure develops, bringing rigid moieties back to the **a** × **c** plane and expanding the parameter **a** to the size of a regular PDI monolayer, in consistency with the gradual geometry change observed (see Figure S14 in SI). For all cases, the few visible reflections and molecular volumes are compatible with an orthorhombic phase of similar nature. The structural parameters have been reported in Table 2.

Putting together all structural information gathered in this study, one can propose two different packing schemes of AD dyads and the ADA triad, illustrated in Figure 8. As a convention, the **a**, **b**, and **c** axes of the unit cell are oriented along the alkyl side chains of the donor group, the π-stacking of the PDI, and the long molecular axis of the AD molecules, respectively. Considering the first model in Figure 8a, the AD molecules are π-stacked into pairs with a strong π-overlap of both the PDI and the donor groups. Donor blocks in successive layers along the **a** axis are pointing alternatively along **c** and −**c**. Within such AD pairs, the solubilizing chains of the two donor blocks are rejected on either side of the conjugated skeleton, and all alkyl chains are grouped together. Figure 8b shows an alternative packing for which the AD molecules are π-stacked into pairs of two molecules with a strong overlap of the PDI units only, whereas donor blocks are arranged side-by-side with the alkyl side chains rejected on each side of the donor pair. However, as for the first model, dense planes of π-stacked PDI blocks are formed also for this molecular arrangement. It is likely that the stacking of PDI units involves a slight lateral offset (arrangement already observed in other studies[27b,30]). However, the PDI long axes are still colinear. These two packing schemes can apply for AD_0, AD_{0T}, and AD_1 dyads. The two different packing schemes in Figure 8a,b can also apply for ADA as illustrated in Figure 8c,d. The two terminal PDI groups on each side of the donor block in ADA can π-stack efficiently without perturbing the packing of donor blocks and can respect the different sectional areas of the two blocks. However, the major difference between AD_n dyads and the ADA triad is the strong interdigitation of the layers of ADA molecules. It can be anticipated that this strong interdigitation is responsible for the enhanced long-range lamellar ordering in ADA films even in the absence of melt-cooling. As a matter of fact, the strong interdigitation of PDI groups on both sides of the donor could partly explain the higher density (1.21 g·cm^{-3}) for the ADA triad compared to the AD_n analogues (1.13−1.14 g·cm^{-3}).

Regarding the D_nAD_n triads, the large sectional area of donor blocks imposes a high molecular area per PDI group which is incompatible with the generation of dense PDI layers. In some sense, the DAD self-assembling into a lamellar structure at long-range order is prevented by the presence of solubilizing ethylhexyl side chains on the donor block that are responsible for the high sectional area of this block as compared to PDI (Figure 8e). The marked discrepancy between molecular areas of D and A segments could similarly be held as responsible for the lack of formation of well-defined D/A segregated structure in other peryleneimide-donor systems.[13c,31,32] Note that the few published examples of well-defined lamellar mesophases in DAD triads (with A = PDI) should be attributed to the presence of a high density of chains (aliphatic[13a] or siloxane[13g]) at the triad extremities, which generates microphase separation.

To conclude, a packing of DAD molecules following a scheme similar to that given in Figure 8 for the AD dyads or the ADA triad is virtually impossible. A more precise structure determination is needed for discriminating one or the other packing behavior of the molecules. Further studies are being undertaken in order to provide a more complete assessment of the molecular packing of AD and ADA molecules.

3. CONCLUSIONS

We have successfully synthesized and characterized a new series of donor−acceptor block co-oligomers with different molecular architectures (AD, DAD, and ADA) with the aim of correlating molecular architecture and self-assembling properties, which is essential to improve optoelectronic devices such as OPV cells or OFET. First, short ethylene linkers have been systematically inserted between the A and D blocks to favor their respective packing. Second, we have verified that these co-oligomers comply with favorable optoelectronic properties, e.g. broad range of absorption, appropriate HOMO and LUMO levels, decoupling of A and D electronic states. This was possible by a careful chemical design of the donor block made of a combination of thienofluorene segments of two different lengths (D_0 or D_1) with the electron-deficient benzothiadiazole unit. Efficient optoelectronic devices require ordered structures with well-segregated acceptor and donor domains that are indeed determined by the molecular architecture. Intensive characterization of the co-oligomers by X-ray diffraction and TEM gave evidence for lamellar mesophases with long-range order after melt-cooling for all systems except for DAD triads. Regardless of the length and chemical nature of the donor block (D_0, D_{0T}, and D_1), all the AD dyads and the ADA triad show very similar packing of the co-oligomers within lamellae.

The major difference between these two systems is the interdigitated character of the lamellae for ADA, which is absent for AD, and results in enhanced long-range ordering in both pristine and melt-cooled ADA films. In the end, AD and ADA superstructures contain extended rows of PDI-stacks within lamellae, leading to three-dimensional mesophases, while DAD systems show short-range lamellar correlations without marked PDI-stacks. The difference in this behavior is explained by the discrepancy of the molecular cross sections between the PDI and the donor blocks. Placing the PDI unit at the end of the molecules allows to compensate its smaller cross-section by the

dx.doi.org/10.1021/ja4129108 | J. Am. Chem. Soc. 2014, 136, 5981−5992

formation of interdigitated rows of PDI-stacks, ultimately leading to the cohesion of the lamellae. In contrast, with the DAD architecture, the large cross-section of the donor blocks prevents the central PDI unit from stacking.

Another important aspect of the preparation of optoelectronic devices is the control of the orientation of the nanostructure. In this work, we have evidenced the influence of the donor block length on the orientation of the lamellar domains on a SiO_2 substrate after melt-cooling. A majority of lying lamellae has been obtained for the short donor blocks (AD_0 and AD_{0T}), whereas AD_1 molecules led to edge-on lamellae. In consequence, the modulation of the block length might be an efficient tool to control the orientation of the oligomers on a substrate, depending on the optoelectronic application (OPV vs OFETs).

Taken all together, these results are important as they allow us to set some basic principles for the molecular design of efficient self-assembling PDI-based donor−acceptor co-oligomers to be used in monocomponent optoelectronic devices.

■ ASSOCIATED CONTENT

Ⓢ Supporting Information

Detailed synthetic procedures, ^1H NMR, ^{13}C NMR, TGA, and MS spectra of final co-oligomers, UV−vis absorption and fluorescence spectra in solution, cyclic voltammetry traces, XRD patterns of ADA as a function of the temperature, ED-patterns and BF-TEM images of D_0AD_0. This material is available free of charge via the Internet at http://pubs.acs.org.

■ AUTHOR INFORMATION

Corresponding Author

stephane.mery@ipcms.unistra.fr

Notes

The authors declare no competing financial interest.

■ ACKNOWLEDGMENTS

This work has been supported by the French National Research Agency (ANR PICASSO Project) and by the European Community via the Interreg IV-A program (C25, Rhin-Solar). We thank Pohang Accelerator Laboratory (PAL) for giving us the opportunity to perform the GIWAXS measurements, MEST and POSTECH for supporting these experiments, Dr. Tae Joo Shin for adjustments and help, and other people from 9A U-SAXS beamline for assistance.

■ REFERENCES

(1) Chen, J. T.; Hsu, C.-S. *Polym. Chem.* **2011**, *2*, 2707−2722.
(2) Liu, H.; Xu, J.; Li, Y.; Li, Y. *Acc. Chem. Res.* **2010**, *43*, 1496−1508.
(3) Hoeben, F. J. M.; Jonkhejim; Meijer, E. W.; Schenning, A. P. H. J. *Chem. Rev.* **2005**, *105*, 1491−1546.
(4) Coakley, K. M.; McGehee, M. D. *Chem. Mater.* **2004**, *16*, 4533−4542.
(5) Hoppe, H.; Sariciftci, N. S. *Adv. Polym. Sci.* **2008**, *214*, 1−86.
(6) Yang, X.; Loos, J. *Macromolecules* **2007**, *40*, 1353−1362.
(7) Thompson, B. C.; Fréchet, J. M. J. *Angew. Chem., Int. Ed.* **2008**, *47*, 58−77.
(8) (a) De Boer, B.; Stalmach, U.; Melzer, C.; Krasnikov, V. V.; Hadziioannou, G. *Polymer* **2001**, *43*, 9097−9109. (b) Zhang, F.; Svensson, M.; Andersson, M. R.; Maggini, M.; Bucella, S.; Menna, E.; Ingänas, O. *Adv. Mater.* **2001**, *13*, 1871−1874. (c) Miyanishi, S.; Zhang, Y.; Tajima, K.; Hashimoto, K. *Chem. Commun.* **2010**, *46*, 6723−6725. (d) Lindner, S. M.; Thelakkat, M. *Macromolecules* **2004**, *37*, 8832−8835. (e) Sommer, M.; Huettner, S.; Thelakkat, M. *J. Mater. Chem.* **2010**, *20*, 10788−10797. (f) Zhang, Q.; Cirpan, A.; Russel, T. P.; Emrick, T. *Macromolecules* **2009**, *42*, 1079−1082. (g) Sommer, M.; Lindner, S. M.; Thelakkat, M. *Adv. Funct. Mater.* **2007**, *17*, 1493−1500. (h) Lohwasser, R. H.; Gupta, G.; Kohn, P.; Sommer, M.; Lang, A. S.; Thurn-Albrecht, T.; Thelakkat, M. *Macromolecules* **2013**, *46*, 4403−4410.
(9) (a) Nierengarten, J.-F. *Sol. Energy Mater. Sol. Cells* **2004**, *83*, 187−199. (b) Roncali, J. *Chem. Soc. Rev.* **2005**, *34*, 483−495. (c) Segura, J. L.; Martin, N.; Guldi, D. M. *Chem. Soc. Rev.* **2005**, *34*, 31−47.
(10) (a) Würthner, F.; Chen, Z.; Hoeben, F. J. M.; Osswald, P.; You, C.-C.; Jonkheijm, P.; van Herrikhuyzen, J.; Schenning, A. P. H. J.; van der Schoot, P. P. A. M.; Meijer, E. W.; Beckers, E. H. A.; Meskers, S. C. J.; Janssen, R. A. J. *J. Am. Chem. Soc.* **2004**, *126*, 10611−10618. (b) Ramos, A. M.; Meskers, S. C. J.; Beckers, E. H. A.; Prince, R. B.; Brunsveld, L.; Janssen, R. A. J. *J. Am. Chem. Soc.* **2004**, *126*, 9630−9644. (c) Bu, L.; Guo, X.; Yu, B.; Qu, Y.; Xie, Z.; Yan, D.; Geng, Y.; Wang, F. *J. Am. Chem. Soc.* **2009**, *131*, 13242−13243. (d) Bu, l.; Guo, X.; Yu, B.; Fu, Y.; Qu, Y.; Xie, Z.; Yan, D.; Geng, Y.; Wang, F. *Polymer* **2011**, *52*, 4253−4260.
(11) (a) Nierengarten, J.-F.; Eckert, J.-F.; Nicoud, J.-F.; Ouali, L.; Krasnikov, V.; Hadziioannou, G. *Chem. Commun.* **1999**, 617−618. (b) Li, W. S.; Yamamoto, Y.; Fukushima, T.; Saeki, A.; Seki, S.; Tagawa, S.; Masunaga, H.; Sasaki, S.; Takata, M.; Aida, T. *J. Am. Chem. Soc.* **2008**, *130*, 8886−8887. (c) Nishizawa, T.; Tajima, K.; Hashimoto, K. *J. Mater. Chem.* **2007**, *17*, 2440−2445. (d) Nishizawa, T.; Tajima, K.; Hashimoto, K. *Nanotechnology* **2008**, *19*, 424017.
(12) (a) Chen, L. X.; Xiao, S.; Yu, L. *J. Phys. Chem. B* **2006**, *110*, 111730−11738. (b) Cremer, J.; Mena-Osteritz, E.; Pschirere, N. G.; Müllen, K.; Bäuerle, P. *Org. Biomol. Chem.* **2005**, *3*, 985−995. (c) Cremer, J.; Bäuerle, P. *Eur. J. Org. Chem.* **2005**, 3715−3723. (d) Cremer, J.; Bäuerle, P. *J. Mater. Chem.* **2006**, *16*, 874−884. (e) Bullock, J. E.; Carmieli, R.; Mickley, S. M.; Vura-Weis, J.; Wasielewski, M. *J. Am. Chem. Soc.* **2009**, *131*, 11919−11929. (f) Balaji, G.; Kale, T. S.; Keerty, A.; Della Pelle, A. M.; Thayumanavan, S.; Valliyaveettil, S. *Org. Lett.* **2011**, *13*, 18−21.
(13) (a) Peeters, E.; van Hal, P. A.; Meskers, S. C. J.; Janssen, R. J. A.; Meijer, E. W. *Chem.—Eur. J.* **2002**, *8*, 4470−4474. (b) van der Boom, T.; Hayes, R. T.; Zhao, Y.; Bushard, P. J.; Weiss, E. A.; Wasielewski, M. R. *J. Am. Chem. Soc.* **2002**, *124*, 9582−9590. (c) Dössel, L. F.; Kamm, V.; Hoiward, I. A.; Laquai, F.; Pisula, W.; Feng, X.; Li, C.; Takase, M.; Kudernac, T.; de Feyter, S.; Müllen, K. *J. Am. Chem. Soc.* **2012**, *134*, 5876−5886. (d) Kim, M. H.; Cho, M. J.; Kim, K. H.; Hoang, M. H.; Lee, T. W.; Jin, J.-I.; Kang, N. S.; Yu, J.-W.; Choi, D. H. *Org. Electron.* **2009**, *10*, 1429−1441. (e) Jonkheijm, P.; Stutzmann, N.; Chen, Z.; de Leeuw, D. M.; Meijer, E. W.; Schenning, A. P. H. J.; Würthner, F. *J. Am. Chem. Soc.* **2006**, *128*, 9535−9540. (f) Mativestsky, J. M.; Kastler, M.; Savage, R. C.; Gentilini, D.; Palma, M.; Pisula, W.; Müllen, K.; Samori, P. *Adv. Funct. Mater.* **2009**, *19*, 2486−2494. (g) Roland, T.; Léonard, J.; Hernandez Ramirez, G.; Méry, S.; Yurchenko, O.; Ludwigs, S.; Haacke, S. *Phys. Chem. Chem. Phys.* **2012**, *14*, 273−279.
(14) Kim, M. S.; Kim, J. S.; Cho, J. C.; Shtein, M.; Guo, L. J.; Kim, J. *Appl. Phys. Lett.* **2007**, *90*, 123113.
(15) (a) Fisslthaler, E.; Blümel, A.; Landfester, K.; Scherf, U.; List, E J W. *Soft Matter* **2008**, *4*, 2448−2453. (b) Kim, H.-C.; Park, S.-M.; Hinsberg, W. D. *Chem. Rev.* **2010**, *110*, 146−177. (c) He, X.; Gao, F.; Tu, G.; Hasko, D. G.; Hüttner, S.; Greenham, N. C.; Steiner, U.; Friend, R. H.; Huck, W. T. S. *Adv. Funct. Mater.* **2011**, *21*, 139−146.
(16) (a) Mishra, A.; MA, C.-Q.; Bäuerle, P. *Chem. Rev.* **2009**, *109*, 1141−1276. (b) Yassar, A.; Miozzo, L.; Gironda, R.; Horowitz, G. *Prog. Polym. Sci.* **2013**, *38*, 791−844. (c) Kozma, E.; Catellani, M. *Dyes Pigments* **2013**, *98*, 160−179. (d) Sommer, M.; Huettner, S.; Thelakkat, M. *Adv. Polym. Sci.* **2010**, *228*, 123−153.
(17) (a) Würthner, F. *Chem. Commun.* **2004**, 1564−1579. (b) Zhan, X.; Facchetti, A.; Barlow, S.; Marks, T. J.; Ratner, M. A.; Wasielewski, M. R.; Marder, S. R. *Adv. Mater.* **2011**, *23*, 268−284. (c) Li, C.; Wonneberger, H. *Adv. Mater.* **2012**, *24*, 613−636. (d) Kozma, E.; Catellani, M. *Dyes Pigments* **2013**, *98*, 160−179.
(18) (a) Richard, F.; Brochon, C.; Leclerc, N.; Eckhardt, D.; Heiser, T.; Hadziioannou, G. *Macromol. Rapid Commun.* **2008**, *29*, 885−891.

(b) Yassar, A.; Miozzo, L.; Gironda, R.; Horowitz, G. *Prog. Polym. Sci.* **2013**, *38*, 791−844.
(19) (a) Samori, P.; Yin, X.; Tchebotareva, N.; Wang, Z.; Pakula, T.; Jäckel, F.; Watson, M. D.; Venturini, A.; Müllen, K.; Rabe, J. R. *J. Am. Chem. Soc.* **2004**, *126*, 3567−3575. (b) Yamamoto, Y.; Fukushima, T.; Suna, Y.; Ishii, N.; Saeki, A.; Seki, S.; Tagawa, S.; Taniguchi, M.; Kawai, T.; Aida, T. *Science* **2006**, *314*, 1761−1764.
(20) (a) Langhals, H. *Helv. Chim. Acta* **2005**, *88*, 1309−1343. (b) Vura-Weis, J.; Ratner, M. A.; Wasielewski, M. R. *J. Am. Chem. Soc.* **2010**, *132*, 1738−1739.
(21) (a) Grell, M.; Bradley, D. D. C.; Inbasekaran, M.; Woo, E. P. *Adv. Mater.* **1997**, *9*, 798. (b) Sherf, U.; List, E. J. W. *Adv. Mater.* **2002**, *14*, 477−487. Zhang, X.; Qu, Y.; Bu, L.; Tian, H.; Zhang, J.; Wang, L.; Geng, Y.; Wang, F. *Chem.—Eur. J.* **2007**, *13*, 5238−6248.
(22) (a) Biniek, L.; Fall, S.; Chochos, C. L.; Leclerc, N.; Lévêque, P.; Heiser, T. *Org. Electron.* **2012**, *13*, 114−120. (b) Schwartz, P. O.; Zaborova, E.; Bechara, R.; Lévêque, P.; Heiser, T.; Méry, S.; Leclerc, N. *New J. Chem.* **2013**, *37*, 2317−2323.
(23) Ramos, A. M.; Beckers, E. H. A.; Offermans, T.; Meskers, S. C. J.; Janssen, R. A. J. *J. Phys. Chem. A* **2004**, *108*, 8201−8211.
(24) (a) Biniek, L.; Fall, S.; Chochos, C. L.; Anokhin, D. V.; Ivanov, D.; Leclerc, N.; Lévêque, P.; Heiser, T. *Macromolecules* **2010**, *43*, 9779−9786. (b) Chu, T.-Y.; Lu, J.; Beaupré, S.; Zhang, Y.; Pouliot, P.-R.; Zhou, J.; Najari, A.; Leclerc, M.; Tao, Y. *Adv. Funct. Mater.* **2012**, *22*, 2345−2351.
(25) Kelber, J.; Bock, H.; Thiebaut, O.; Grelet, E.; Langhals, H. *Eur. J. Org. Chem.* **2011**, 707−712.
(26) Baek, M.-J.; Jang, W.; Lee, S.-H.; Lee, Y.-S. *Synth. Met.* **2012**, *161*, 2785−2791.
(27) (a) Hansen, M. R.; Graf, R.; Sekharan, S.; Sebastiani, D. *J. Am. Chem. Soc.* **2009**, *131*, 5251−5256. (b) Struijk, C. W.; Sieval, A. B.; Dackorst, J. E. J.; van Dijk, M.; Kimbes, P.; Koehorst, R. B. M.; Donker, H.; Schaafsma, T. J.; Picken, S. J.; van de Craats, A. M.; Warman, J. M.; Zuilhof, H.; Sudholter, E. J. R. *J. Am. Chem. Soc.* **2000**, *122*, 11057−11066.
(28) For instance in the structure DICLIK (*N*,*N*′-diethylperylene-3,4:9,10-bis(dicarboximide)) from the Cambridge Structural Database.
(29) From the estimated partial volume expansion with respect to crystal.
(30) Kazmaier, P. M.; Hoffmann, R. *J. Am. Chem. Soc.* **1994**, *116*, 9684−9691.
(31) Neuteboom, E. E.; Meskers, S. C. J.; van Hal, P. A.; van Duren, J. K. J.; Meijer, E. W.; Janssen, R. A. J.; Dupin, H.; Pourois, G.; Cornil, J.; Lazzaroni, R.; Brédas, J.-L.; Beljonne, D. *J. Am. Chem. Soc.* **2003**, *125*, 8625−8638.
(32) Pron, A.; Reghu, R. R.; Rybakiewicz, R.; Cybulski, H.; Djurado, D.; Grazulevicius, J. V.; Zagorska, M.; Kulszewicz-Bajer, I.; Verilhac, J.-M. *J. Phys. Chem. C* **2011**, *115*, 15008−15017.